scientific reports

Check for updates

OPEN

# Exploiting silver ions' antimicrobial properties for colorimetric detection of *Salmonella* via suppressed formation of Au@Ag nanorods

Sobhan Soleimani[1,2], Amir Hossein Q. Selakjan[1], Forough Ghasemi[1]✉, Ehsan Shokri[1], Peyman Kheirandish Zarandi[1] & Mahdi Alijanianzadeh[2]

***Salmonella typhimurium*, a leading cause of global foodborne illness, demands rapid, on-site detection to combat its widespread contamination in food supplies—where delayed diagnosis contributes to thousands of annual fatalities. Here, we present a novel colorimetric biosensing platform that exploits the intrinsic antimicrobial properties of silver ions ($Ag^+$) to enable instrument-free, visual quantification of *Salmonella typhimurium*. The sensor relies on the controlled growth of gold@silver core–shell nanorods (Au@AgNRs), whose localized surface plasmon resonance (LSPR) peak undergoes a vivid, concentration-dependent color shift as silver shell deposition modulates their aspect ratio. In the absence of bacteria, $Ag^+$ ions are reduced by ascorbic acid (AA) and uniformly coat AuNRs, inducing a blue shift. However, when *Salmonella typhimurium* is present, bacterial cells sequester $Ag^+$ through interactions with surface biomolecules, inhibiting complete shell formation and resulting in a measurable red shift in the LSPR peak accompanied by visually discernible color transitions from red to magenta, purple, violet, dark blue, and teal. The system achieves a linear dynamic range of $18.75 \times 10^6$ to $112.5 \times 10^6$ CFU $mL^{-1}$ and a limit of detection (LOD) of $2.0 \times 10^6$ CFU $mL^{-1}$. Prior to detection, target bacteria are isolated from complex matrices using anti-Salmonella aptamer-conjugated magnetic nanoparticles (MNPs), ensuring specificity and minimizing matrix interference. Successful validation in spiked chicken bouillon samples (recovery: 93.3%, RSD: 3.5%) confirms practical utility under real-world conditions. This strategy uniquely merges microbiology with nanomaterials science, offering a low-cost, rapid, and visually interpretable solution for decentralized pathogen screening.**

**Keywords** Salmonella detection, Anti-formation mechanism, Gold@silver nanorods, Colorimetric sensor

*Salmonella*, a Gram-negative bacterium belonging to the Enterobacteriaceae family, is among the most prevalent etiological agents of foodborne illness worldwide, with over 2,500 identified serotypes[1]. Human infections, collectively termed salmonellosis, typically manifest as acute gastroenteritis but can progress to life-threatening systemic conditions such as bacteremia and typhoid fever[2]. Transmission occurs primarily via the fecal–oral route[3], including consumption of contaminated water[4] or crops irrigated with wastewater. Alarmingly, *Salmonella* exhibits remarkable environmental persistence, particularly in low-moisture foods such as spices[5], chocolate[6], dried milk[7], and peanut butter[8], where it can survive for months. According to the World Health Organization, diarrheal diseases—for which *Salmonella* is a leading contributor—affect approximately 550 million people annually and result in nearly 42,000 deaths[9,10]. The infectious dose varies significantly depending on the bacterial strain, host susceptibility, and food matrix[11], underscoring the need for sensitive, rapid, and field-deployable detection methods to mitigate outbreaks and reduce mortality.

Current detection approaches include traditional culture-based methods[12], miniaturized biochemical assays[13], immunoassays (e.g., ELISA[14], latex agglutination[15], nucleic acid amplification techniques (e.g., PCR[16],

[1]Department of Nanotechnology, Agricultural Research, Education, and Extension Organization (AREEO), Agricultural Biotechnology Research Institute of Iran (ABRII), Karaj, Iran. [2]Department of Cell and Molecular Biology, Faculty of Biological Sciences, Kharazmi University, Tehran, Iran. ✉email: forough.ghasemi@abrii.ac.ir

hybridization[17], CRISPR-based systems[18], Raman spectroscopy[19], phage-based detection[20], biosensors[21], and microfluidic platforms[22]. While effective in controlled settings, these methods often suffer from prolonged analysis times, high costs, requirement for specialized equipment or trained personnel, and limited suitability for on-site applications. To address these limitations, plasmonic nanoparticles—particularly gold (AuNPs) and silver (AgNPs)—have emerged as powerful transducers in colorimetric sensing due to their strong, tunable optical responses governed by localized surface plasmon resonance (LSPR)[23–26]. LSPR arises from the collective oscillation of conduction electrons upon light excitation, resulting in intense light scattering and absorption in the visible spectrum[27–32]. Critically, the LSPR wavelength is exquisitely sensitive to nanoparticle size, shape, composition, and local dielectric environment[33].

Among plasmonic nanostructures, gold nanorods (AuNRs) are particularly advantageous due to their dual LSPR peaks: a transverse mode (~ 520 nm) and a longitudinal mode that can be precisely tuned across the visible to near-infrared range by modulating the aspect ratio[34,35]. A reduction in aspect ratio—for instance, via conformal silver shell growth to form Au@Ag core–shell nanorods—induces a pronounced blue shift in the longitudinal peak[36]. This phenomenon has been leveraged for multicolor sensing applications[37–43]. Simultaneously, silver ions ($Ag^+$) are well-established antimicrobial agents, exerting their effects through interactions with vital cellular components, including thiol-containing proteins, respiratory enzymes, and nucleic acids[44–46]. These interactions disrupt microbial metabolism, inhibit ATP synthesis, and induce oxidative stress. In this work, we introduce a novel sensing paradigm that strategically exploits this antimicrobial activity for analytical purposes.

For the first time, we demonstrate that *Salmonella typhimurium* can be detected by its ability to sequester $Ag^+$ ions, thereby inhibiting the formation of Au@Ag core–shell nanorods. This "anti-formation" mechanism results in a concentration-dependent red shift of the LSPR peak, accompanied by visually discernible color transitions—from red to magenta, purple, violet, dark blue, and teal—enabling semi-quantitative, instrument-free readout (Fig. 1). Prior to detection, target bacteria are selectively captured from complex samples using commercially available anti-Salmonella aptamer-functionalized magnetic nanoparticles (MNPs), ensuring high specificity and compatibility with real-world matrices (Fig. 2). This approach represents a significant conceptual and practical advance: it transforms a biological defense mechanism into a quantifiable optical signal, eliminating the need for enzymatic amplification, antibody labeling, or sophisticated instrumentation. The result is a robust and user-friendly platform ideally suited for point-of-need applications in resource-limited settings.

## Materials and methods

### Materials

Hydrogen tetrachloroaurate(III) ($HAuCl_4.3H_2O$), 5-bromo-2-hydroxybenzoic acid (5-BrSA), sodium borohydride ($NaBH_4$), cetyltrimethylammonium bromide (CTAB), ascorbic acid (AA), silver nitrate ($AgNO_3$), 2-(n-morpholino) ethane sulfonic acid (MES), luciferase and luciferin were obtained from Sigma-Aldrich. *Salmonella enterica subsp. enterica serovar Typhimurium* (ATCC 14028) was prepared from Iran Scientific-Industrial Research Center. All microbial culture media and components include tryptic soy broth (TSB), nutrient broth, peptone, and agar were purchased from Merck.

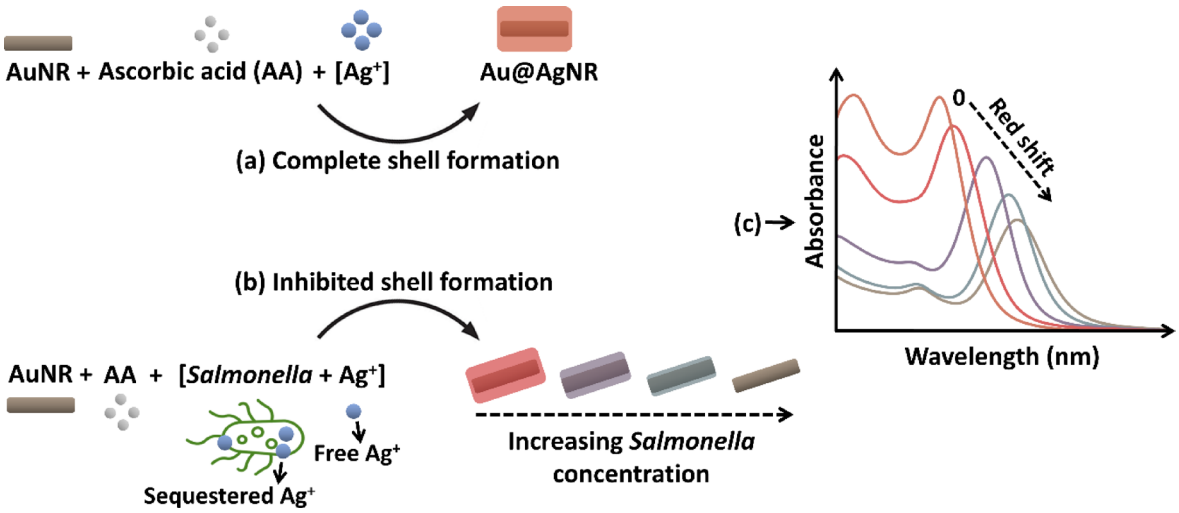


**Fig. 1**. Schematic representation of the colorimetric sensing mechanism based on the inhibition of Au@Ag core-shell nanorod (Au@AgNR) formation by *Salmonella typhimurium*. (**a**) In the absence of bacteria, ascorbic acid (AA) reduces free silver ions ($Ag^+$) to metallic silver ($Ag^0$), which deposits uniformly around gold nanorods (AuNRs) to form complete Au@AgNRs. (**b**) In the presence of *Salmonella*, bacterial cells sequester free $Ag^+$ ions via interactions with surface biomolecules, reducing their availability for reduction and thereby inhibiting the formation of a complete Ag shell on the AuNRs. This results in incomplete or thinner coatings. (**c**) This inhibition leads to a concentration-dependent increase in the aspect ratio of the resulting nanostructures, causing a red shift in the localized surface plasmon resonance (LSPR) peak, as demonstrated by the spectral shift in the UV-Vis absorption profiles.

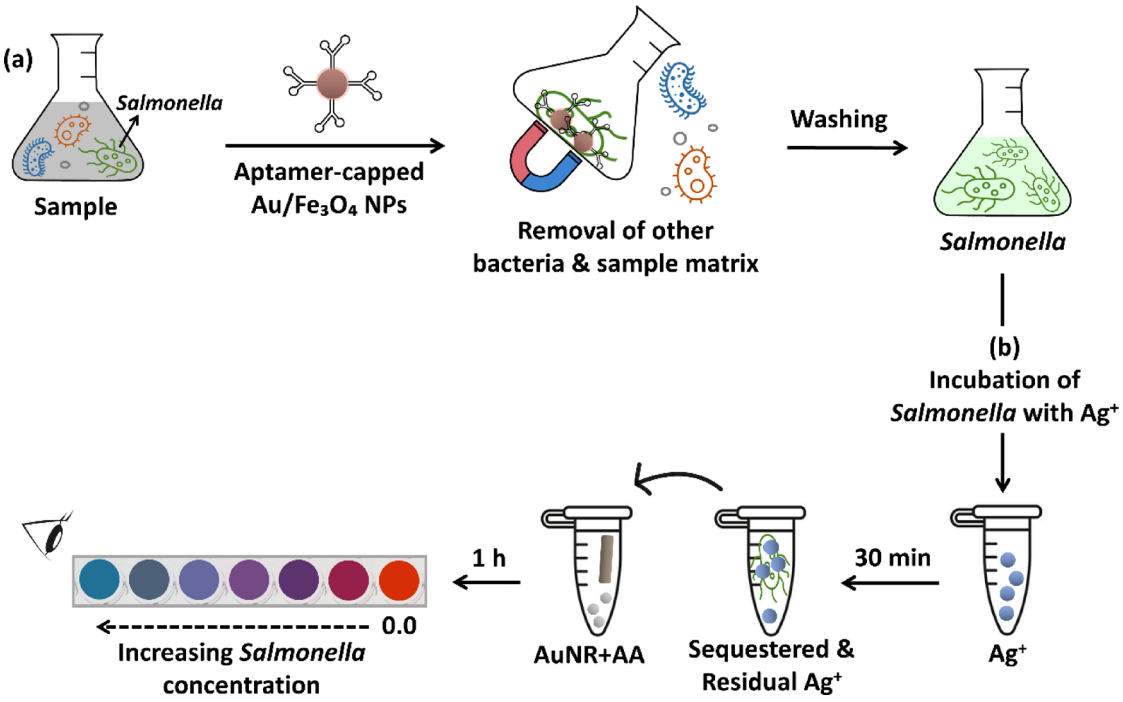


**Fig. 2**. Schematic illustration of the two-step protocol for detecting *Salmonella typhimurium* using aptamer-functionalized magnetic nanoparticles and the designed colorimetric sensor. (**a**) Immunomagnetic separation: Aptamer-capped Au/$Fe_3O_4$ nanoparticles selectively bind *Salmonella* cells from a complex sample containing other bacteria and matrix components. A magnet is used to isolate the nanoparticle-bacteria complexes, while unbound contaminants are removed by washing. (**b**) Colorimetric detection: Isolated *Salmonella* cells sequester silver ions ($Ag^+$) via surface interactions. The residual, unbound $Ag^+$ is then reduced by ascorbic acid (AA) in the presence of gold nanorods (AuNRs), leading to the formation of Au@Ag core-shell nanostructures. This process induces a concentration-dependent color shift (from red to teal) that can be visually interpreted without instrumentation.

## Instrumentation

A Lambda (PerkinElmer, USA) spectrophotometer was used for absorbance spectral recording at room temperature. To determine the size of the nanoparticles, a PHILIPS MC 10 TH microscope was used recording the transmission electron microscopy (TEM) images at an accelerating voltage of 100 kV. The color images were captured using a Samsung Galaxy a73 smartphone.

## Synthesis of AuNRs

Gold nanorods were synthesized through a previously reported seed-mediated approach with a few alterations[47]. Firstly, 0.125 mL of $HAuCl_4$ (0.01 mol $L^{-1}$) and then, 0.30 mL of fresh $NaBH_4$ (0.01 mol $L^{-1}$) were added to 4.7 mL of CTAB solution (0.10 mol $L^{-1}$) to prepare the seed solution. At this point, the tint of the solution started to change from yellow to brownish-yellow within a min. Afterward, the solution was stirred for 2 h at room temperature. To prepare AuNRs, 50 mg of 5-BrSA was added to 25.0 mL of 0.1 mol $L^{-1}$ CTAB solution and dissolved. Then, 480 µL of 0.01 mol $L^{-1}$ $AgNO_3$ was mixed with the solution and mildly stirred for 15 min at room temperature. Subsequently, 25.0 mL of 0.001 mol $L^{-1}$ $HAuCl_4$ solution was added to the mixture. After 120 min of pre-reduction, 130 µL of 0.1 mol $L^{-1}$ ascorbic acid solution was added under vigorous stirring. Eventually, 80 µL of the seed solution was injected into the growth solution and the stirring was stopped after 30 s. The mixture was left undisturbed at room temperature for at least 4 h to gradually change its color to brown. The synthesized AuNRs were centrifuged for 10 min at 10,000 rpm. After removing the supernatant, the AuNRs were redispersed in 0.05 mol $L^{-1}$ CTAB.

## Bacterial culture

*Salmonella typhimurium* (ATCC 14028) was revived from stock by inoculating tryptic soy broth (TSB) and incubating overnight at 37 °C. A single colony from the resulting culture was then transferred to fresh TSB and grown for 4 h at 37 °C to obtain mid-log phase cells. The optical density ($OD_{600}$) of the culture was measured using a UV–Vis spectrophotometer, and cultures with an $OD_{600}$ between 0.5 and 0.6 were selected for sensor experiments.

## Sensing procedure

First, bacterial suspensions at varying concentrations were incubated with $AgNO_3$ (final concentration: 300 µmol $L^{-1}$) for 30 min to allow *Salmonella typhimurium* to sequester free $Ag^+$ ions via surface interactions (Fig. 2b).

Subsequently, this mixture was added to a reaction solution containing 0.15 mL of AuNRs, 10 mmol $L^{-1}$ MES buffer (pH 7.0), and 200 µmol $L^{-1}$ ascorbic acid, bringing the total volume to 1.0 mL. The mixture was vortexed vigorously to initiate the reduction of $Ag^+$ to $Ag^0$ and the subsequent growth of the silver shell on the AuNRs. After 60 min of incubation at room temperature, the resulting colorimetric response was quantified by recording UV–Vis absorbance spectra across the range of 400–800 nm.

All measurements were performed in triplicate ($n = 3$), and data are presented as mean ± standard deviation. AuNRs demonstrated optical stability for > 12 months when stored at 4 °C in CTAB solution. Commercial MNPs retained full functionality for > 6 months under refrigerated storage. Due to the irreversible nature of the silver reduction and shell growth reaction, each colorimetric assay is designed as a single-use, disposable format.

### Real sample analysis

Anti-Salmonella magnetic nanoparticles (MNPs) with a core–shell structure ($Fe_3O_4$/Au; diameter: 150 nm; saturation magnetization: 10.15 emu/g) were commercially obtained from Fanavar Zist Farma (FZF) Co., Iran. These MNPs were pre-conjugated with anti-Salmonella aptamers by the manufacturer and used directly without further modification to ensure reproducibility.

For pathogen isolation, food samples (25 g) were homogenized in 225 mL buffered peptone water and pre-enriched at 37 °C for 6–8 h. After centrifugation (3,000 × g, 10 min) to remove debris, the supernatant was incubated with 150 µL of MNP suspension per mL of sample under gentle rotation (25 rpm, 30 min, room temperature) to allow target binding. Magnetic separation was then performed using a permanent rack (5 min), followed by three washes with PBS (3 washes, pH 7.4) to eliminate non-specifically bound material (Fig. 2a).

## Results and discussion

### Principles of sensing

Ascorbic acid (AA, $C_6H_8O_6$) serves as a mild and effective reducing agent, capable of reducing silver ions ($Ag^+$) to metallic silver ($Ag^0$) through electron donation (Eq. 1). In the presence of gold nanorods (AuNRs), which act as nucleation sites, the reduced silver atoms preferentially deposit onto the AuNR surface, leading to the controlled formation of an Au@Ag core–shell nanostructure[48]. This shell growth modifies the surface composition, dimensions, and aspect ratio of the original AuNRs, thereby inducing a measurable shift in their localized surface plasmon resonance (LSPR) band.

$$C_6H_8O_6 + 2Ag^+ \rightarrow C_6H_6O_6 + 2Ag^0 + 2H^+ \quad (1)$$

In the present work, the synthesized AuNRs exhibited distinct transverse and longitudinal localized surface plasmon resonance (LSPR) peaks at 525 nm and 760 nm, respectively (Fig. 3a). Upon addition of ascorbic acid (AA) and $Ag^+$ ions, silver atoms were reduced and deposited onto the AuNR surface, forming gold@silver core–shell nanorods (Au@AgNRs). This shell growth increased the nanoparticle aspect ratio, resulting in a pronounced blue shift of the longitudinal LSPR peak (Fig. 3b, black spectrum). Crucially, when *Salmonella typhimurium* was present prior to shell formation, bacterial cells sequestered free $Ag^+$ ions via interactions with surface biomolecules—thereby inhibiting the reduction and deposition of silver onto the AuNR surface. To exploit this phenomenon, we developed a two-solution sensing strategy: one containing *Salmonella typhimurium* pre-incubated with $AgNO_3$(to allow ion sequestration), and the other containing AuNRs, MES buffer, and AA. Upon mixing, the residual unbound $Ag^+$ was insufficient to support complete shell growth, leading to a measurable red shift in the LSPR peak (Fig. 3b, red spectrum) due to suppressed core-shell formation.

TEM images confirmed that Au@AgNRs formed in the absence of bacteria exhibited smaller aspect ratio (Fig. 3c), whereas those formed in the presence of *Salmonella typhimurium* retained a larger aspect ratio indicative of incomplete silver coating (Fig. 3d). These results validate our novel "anti-formation" mechanism—a unique enzyme-free strategy for colorimetric pathogen detection based on inhibition of nanoparticle growth.

Regarding the interaction of silver ions with bacteria, research has revealed multiple mechanisms by which microorganisms respond to $Ag^+$ exposure. In Gram-negative bacteria such as *Salmonella spp.*, a primary defense strategy involves sequestering $Ag^+$ ions within the periplasmic space, thereby preventing their entry into the cytoplasm and subsequent disruption of vital intracellular processes[49]. Additionally, some strains harbor plasmid-encoded resistance systems; for example, *Salmonella typhimurium* carries the pMG101 plasmid, which contains the sil gene cluster encoding nine proteins essential for active efflux and detoxification of silver ions[50]. Beyond these specific resistance mechanisms, $Ag^+$ ions can directly interact with bacterial membranes, leading to inhibition of ATP synthesis, blockade of DNA replication, impairment of ribosomal function, and induction of reactive oxygen species[51]. Bragg and Rainnie demonstrated that $Ag^+$ at concentrations as low as 15 µmol $L^{-1}$ suppresses the oxidation of key metabolic substrates—glucose, glycerol, fumarate, succinate, and lactate—in *E. coli*, while also altering the composition and function of respiratory chain proteins[52]. Furthermore, $Ag^+$ exhibits high affinity for functional groups in biomolecules, including thiol (-SH) moieties in proteins and nitrogenous bases in DNA, disrupting enzyme activity and genetic integrity[45,53–55]. In the context of this study, we propose that the antimicrobial action of $Ag^+$ in our sensing system arises from its selective binding and accumulation within structural components of the *Salmonella* cell wall—potentially via interaction with purine-rich membrane channels or porins—thereby depleting free $Ag^+$ available for reduction and shell formation on AuNRs (Fig. 3d).

### Optimization of key sensing parameters

To improve the system's stability and sensitivity, several crucial factors, i.e., silver nitrate concentration, ascorbic acid concentration, bacteria and silver mixture incubation time, and analysis time were optimized (Fig. 4). The analytical signal was defined as the wavelength shift ($\Delta\lambda = \lambda - \lambda_0$), where $\lambda_0$ is the longitudinal LSPR peak maximum in the absence of bacteria and $\lambda$ is the peak maximum in its presence.

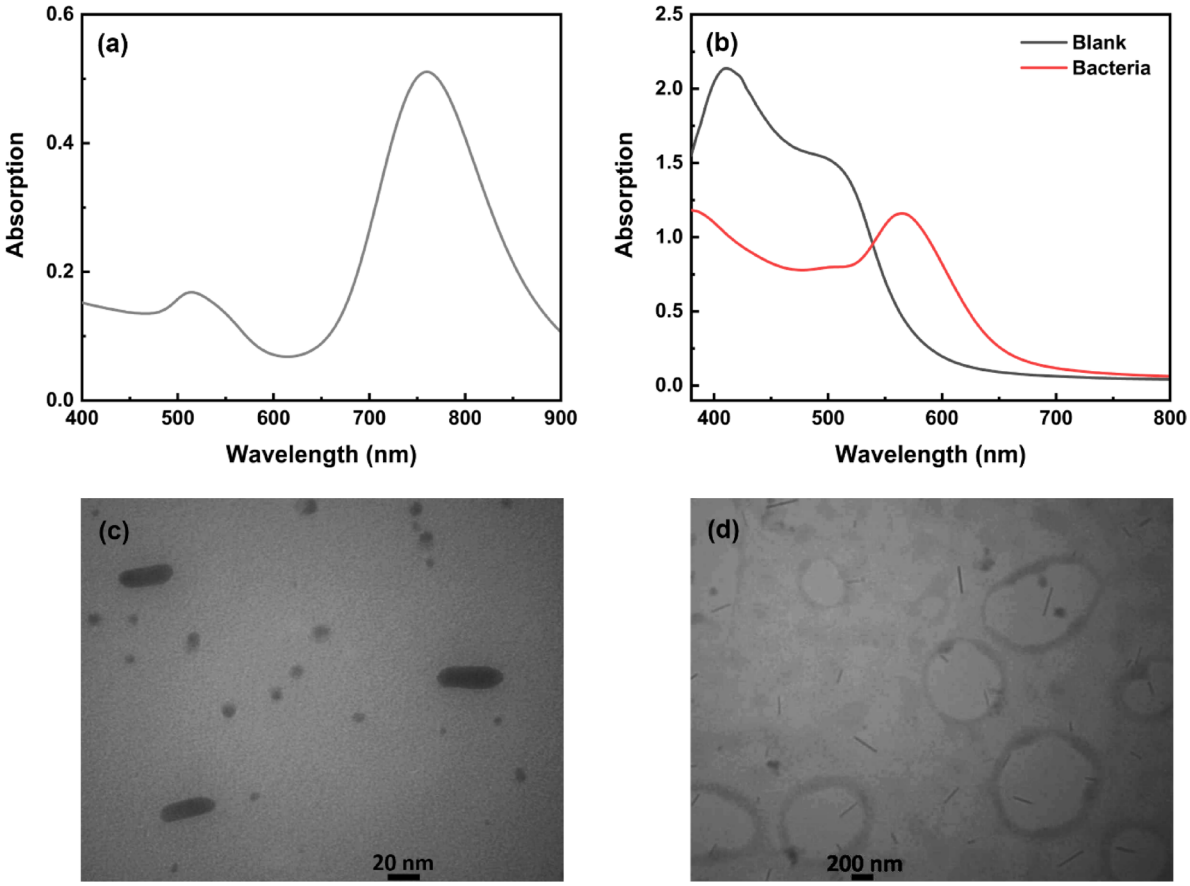


**Fig. 3**. (**a**) UV–Vis absorption spectrum of as-synthesized gold nanorods (AuNRs), showing transverse and longitudinal localized surface plasmon resonance (LSPR) peaks at ~ 525 nm and ~ 760 nm, respectively. (**b**) Absorption spectra of the colorimetric sensor in the absence (black line, blank) and presence (red line) of *Salmonella typhimurium*. The presence of bacteria induces a red shift in the LSPR peak due to inhibition of silver shell formation. Transmission electron microscopy (TEM) images of Au@Ag nanostructures formed (**c**) in the absence of bacteria, showing Au@Ag NRs with uniform silver shells, and (**d**) in the presence of *Salmonella typhimurium*, revealing larger aspect ratio indicative of incomplete shell growth.

*Effect of pH on sensor response*

The reduction of silver ions ($Ag^+$) by ascorbic acid (AA) and the subsequent deposition of metallic silver ($Ag^0$) onto gold nanorods (AuNRs) are fundamentally pH-dependent processes, governed by both thermodynamic and kinetic principles. Simultaneously, the physiological state and surface chemistry of *Salmonella typhimurium*—the target analyte—are profoundly influenced by environmental pH. Therefore, selecting the right assay pH balances the kinetics of the plasmonic transduction with the biological integrity of the target pathogen.

The redox reaction between AA and $Ag^+$ involves proton consumption (Eq. 1), implying that the reaction rate should theoretically increase under alkaline conditions according to Le Chatelier's principle. Based on our preliminary investigations, at pH values above 7.0, we observed rapid, uncontrolled nucleation of $Ag^0$ in solution, leading to the formation of spherical silver nanoparticles (AgNPs) alongside the desired conformal shell growth on AuNRs. This was evidenced by the emergence of a distinct, broad plasmon peak at ~ 400 nm in UV-Vis spectra, characteristic of free AgNPs. These nanoparticles contribute significant background absorption and scattering, obscuring the precise, aspect-ratio-dependent LSPR shift of the Au@AgNRs and drastically reducing the signal-to-noise ratio and reproducibility of the assay.

Conversely, at lower pH values, the reduction kinetics of $Ag^+$ by AA become prohibitively slow. Even in the absence of bacteria, the formation of a complete, uniform silver shell required significantly longer incubation times (> 90 min) to reach optical equilibrium, making the assay impractical for rapid detection. Furthermore, suboptimal pH levels may induce physiological stress or alter the membrane permeability of *Salmonella typhimurium*. While *Salmonella typhimurium* thrives optimally near neutral pH (7.0–7.5), exposure to acidic conditions (pH < 6.5) can trigger its acid tolerance response (ATR), potentially upregulating efflux pumps or altering the expression and accessibility of key surface ligands involved in $Ag^+$ sequestration, such as thiol-containing proteins and lipopolysaccharides (LPS). Such changes could artificially reduce the efficiency of $Ag^+$ binding, leading to an underestimation of bacterial concentration and compromised sensitivity.

Therefore, pH 7.0 was rigorously established as the optimal condition. It enables the controlled formation of Au@AgNRs in the absence of bacteria, while simultaneously preserving the natural $Ag^+$ sequestration capability

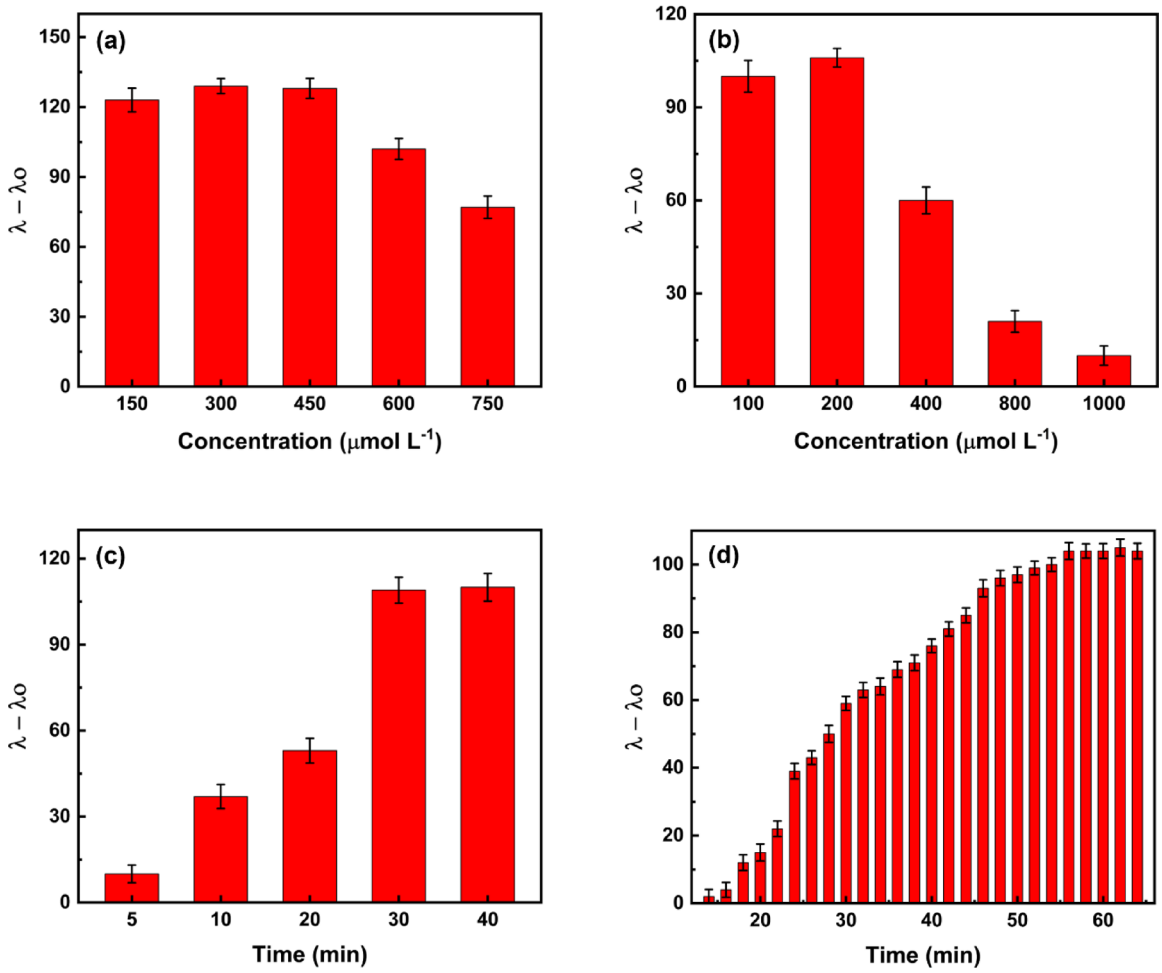


**Fig. 4**. Optimization of key sensing parameters. (**a**) Effect of $AgNO_3$concentration on sensor response (AuNR = 0.15 mL, AA = 200 μmol $L^{-1}$, MES buffer = 50 mmol $L^{-1}$). (**b**) Effect of ascorbic acid concentration on sensor response (AuNR = 0.15 mL, $AgNO_3$= 300 μmol $L^{-1}$, MES buffer = 50 mmol $L^{-1}$, pH 7.0). (c) Influence of incubation time between *Salmonella* and $Ag^+$ ions on sensor response (AuNR = 0.15 mL, $AgNO_3$= 300 μmol $L^{-1}$, AA = 200 μmol $L^{-1}$, MES buffer = 10 mmol $L^{-1}$, pH 7.0). (**d**) Time-dependent evolution of the sensor response after mixing components.

of *Salmonella typhimurium* in its presence. This dual optimization ensures that the observed LSPR red shift is a direct, reliable, and physiologically relevant readout of bacterial load, minimizing artifacts and maximizing analytical fidelity. All subsequent experiments were conducted at this pH to ensure consistency, robustness, and biological relevance.

*Optimization of $Ag^+$ concentration*

In our colorimetric sensing platform, the transduction mechanism relies on the controlled formation of Au@Ag core-shell nanorods (Au@AgNRs) via the reduction of $Ag^+$ ions (from $AgNO_3$) by ascorbic acid (AA) on the surface of gold nanorods (AuNRs). In the absence of bacteria, this process proceeds homogeneously, leading to a uniform silver shell deposition. However, in the presence of *Salmonella typhimurium*, $Ag^+$ ions are competitively sequestered by bacterial surface biomolecules—including thiol (-SH) groups in membrane proteins, lipopolysaccharides, and nucleic acids. This sequestration effectively reduces the concentration of free, reducible $Ag^+$ ions available for shell formation on AuNRs. Consequently, the silver shell becomes thinner or discontinuous, preserving a higher aspect ratio in the resulting nanostructure and leading to red shift—compared to the bacteria-free control.

To rigorously optimize the $Ag^+$ concentration for maximum sensor response, we systematically evaluated five concentrations of $AgNO_3$ (150, 300, 450, 600, and 750 μmol $L^{-1}$) under controlled conditions (Fig. 4a, Figure S1). At low $Ag^+$ concentration (150 μmol $L^{-1}$); the sensor response was suboptimal. The limited availability of $Ag^+$ ions resulted in incomplete shell formation even in the absence of bacteria, yielding a smaller baseline LSPR shift. Consequently, the relative inhibition caused by bacterial sequestration was not in its maximum. At intermediate concentrations (300–450 μmol $L^{-1}$); a significant and reproducible LSPR shift was observed in the absence of bacteria, indicating robust shell formation. In the presence of a fixed concentration of *Salmonella typhimurium*, a pronounced inhibition of this shift occurred, as bacterial cells effectively sequestered a substantial fraction of

the available $Ag^+$. Notably, the responses at 300 and 450 μmol $L^{-1}$ were comparable (**Figure** S1b, c and Fig. 4a), suggesting that within this range, the system operates near its optimal sensitivity—where the amount of $Ag^+$ is sufficient for full shell formation in the control, yet low enough that the bacterial biomass can meaningfully inhibit it. At high concentrations (> 450 μmol $L^{-1}$, i.e., 600 and 750 μmol $L^{-1}$); the sensor response decreased significantly. The excess $Ag^+$ ions overwhelm the sequestration capacity of the bacterial cells. Even after bacterial binding, a large surplus of free $Ag^+$ remains in solution, which is then reduced by AA to form a near-complete silver shell. This diminishes the spectral difference (Δλ) between the "bacteria-present" and "bacteria-absent" samples, thereby reducing the sensor's sensitivity and signal-to-noise ratio.

Although 300 and 450 μmol $L^{-1}$ yielded similar absolute responses, 300 μmol $L^{-1}$ was selected as the optimal concentration for the following refined reasons. (i) At 300 μmol $L^{-1}$, the baseline shift (without bacteria) is sufficiently large for easy detection, while the relative inhibition by bacteria is maximized, leading to the highest contrast between negative and positive signals. (ii) A lower [$Ag^+$] enables detection of lower bacterial concentrations—because even a small number of *Salmonella typhimurium* cells can sequester a significant fraction of the limited $Ag^+$ pool, effectively inhibiting shell formation. This results in a lower limit of detection (LOD) and enhances sensitivity at low pathogen loads, which is critical for early-stage contamination screening. Conversely, higher $Ag^+$ concentrations (e.g., 450 μmol $L^{-1}$) require a much larger bacterial load to achieve comparable inhibition, reducing sensitivity and pushing the LOD upward. Therefore, selecting the minimal effective $Ag^+$ concentration optimizes both sensitivity and practical utility for real-world applications.

*Optimization of ascorbic acid concentration*

Ascorbic acid (AA) serves as the mild, biocompatible reducing agent responsible for the controlled reduction of $Ag^+$ ions to metallic silver ($Ag^0$) on the surface of gold nanorods (AuNRs). The kinetics and spatial control of this reduction are critical. In the presence of *Salmonella typhimurium*, a fraction of $Ag^+$ ions is sequestered by bacterial surface ligands (e.g., -SH, $-NH_2$, $-PO_4^{3-}$), rendering them unavailable for reduction. Therefore, the concentration of AA must be carefully tuned to ensure that: (i) In the absence of bacteria, sufficient reducing power exists to drive complete, uniform Ag shell formation—yielding a large, reproducible LSPR blue shift. (ii) In the presence of bacteria, the reduction process remains sensitive to the decreased availability of free $Ag^+$, resulting in a measurable inhibition of shell growth and a smaller LSPR shift. To achieve this balance, we evaluated five concentrations of AA (100, 200, 400, 800, and 1000 μmol $L^{-1}$) while keeping all other parameters constant (Fig. 4b, Figure S2).

At low AA concentration (100 μmol $L^{-1}$); the reduction kinetics were slow to achieve complete shell formation within the reaction time—even in the absence of bacteria. This resulted in a small baseline LSPR shift and consequently, a weak analytical signal upon bacterial addition. The system was reduction-limited. At optimal concentration (200 μmol $L^{-1}$); the reduction rate was perfectly matched to the experimental timeframe. A complete, uniform Ag shell formed in the absence of bacteria, yielding the maximum possible LSPR blue shift. In the presence of bacteria, sequestration of $Ag^+$ significantly inhibited this process, leading to the largest differential signal—i.e., maximum sensor contrast. At high concentrations (≥ 400 μmol $L^{-1}$); sensor performance degraded progressively. While the baseline LSPR shift (without bacteria) continued to increase slightly, the inhibited signal (with bacteria) decreased. This convergence of signals reduced the net analytical response. At [AA] ≥ 400 μmol $L^{-1}$, nucleation of spherical Ag nanoparticles in solution becomes thermodynamically favorable. This is evident in **Figure S2c-e** by the emergence of a secondary, broad plasmon peak around ~ 400 nm—characteristic of spherical Ag nanoparticles. These free AgNPs contribute to background absorption, increase scattering, and reduce the specificity of the LSPR signal originating from Au@AgNRs.

Concentration 200 μmol $L^{-1}$ was selected as the optimal concentration of AA because: (i) this concentration yielded the largest difference in LSPR shift between "with bacteria" and "without bacteria" conditions—the true measure of sensor sensitivity. (ii) At 200 μmol $L^{-1}$, reduction is predominantly heterogeneous (surface-limited on AuNRs), as confirmed by the absence of a ~ 400 nm AgNP peak in **Figure S2b**. This ensures signal specificity and minimizes background noise.

*Optimization of $Ag^+$–bacteria incubation time*

The incubation time between *Salmonella typhimurium* cells and silver ions ($Ag^+$) is a critical kinetic parameter that governs the efficiency of $Ag^+$ sequestration by bacterial surface biomolecules. As outlined in Sect. 3.1, $Ag^+$ ions interact with multiple cellular targets—including thiol (-SH) groups in membrane proteins, phosphate moieties in lipopolysaccharides (LPS), and nitrogenous bases in exposed DNA—leading to their immobilization within the bacterial envelope. These interactions are not instantaneous; they require sufficient contact time for diffusion, binding, and internalization (or surface complexation) to occur.

To systematically evaluate the impact of incubation duration on sensor performance, we tested five time intervals: 5, 10, 20, 30, and 40 min (**Figure S3**). The sensor response, defined as $\Delta\lambda = \lambda$ (with bacteria) – $\lambda_0$ (without bacteria), exhibited a clear positive correlation with incubation time. This trend is mechanistically intuitive: longer incubation allows more $Ag^+$ ions to interact with a greater number of bacterial binding sites, thereby reducing the pool of free $Ag^+$ available for subsequent reduction and deposition onto AuNRs. Consequently, the inhibition of core–shell formation becomes more pronounced, resulting in a larger red shift in the LSPR peak—and thus a stronger analytical signal. However, the incremental gain in sensor response diminished significantly beyond 30 min. As shown in Fig. 4c, the difference in Δλ between 30 and 40 min was statistically negligible, indicating that the system approaches equilibrium within this timeframe. At 30 min, the majority of accessible binding sites on the bacterial surface are saturated, and further extension of incubation yields minimal additional sequestration. Therefore, 30 min was selected as the optimal incubation time. This choice represents a scientifically justified compromise: it ensures near-maximal $Ag^+$ sequestration (and thus maximal sensor sensitivity) while avoiding unnecessary prolongation of the assay.

*Optimization of reaction analysis time*

Following the incubation and mixing of all components—AuNRs, residual $Ag^+$, ascorbic acid (AA), and MES buffer—the transduction phase of the assay commences: the controlled reduction of free $Ag^+$ ions and their deposition as a metallic silver shell onto the surface of AuNRs. This heterogeneous nucleation and growth process directly modulates the aspect ratio of the nanorods, inducing a visually observable color transition. To ensure that spectral measurements are taken at the point of maximum signal differentiation, we monitored the evolution of the LSPR peak shift over one hour, recording absorbance spectra every 2 min under optimized conditions.

The results, presented in Fig. 4d, reveal that the LSPR shift ($\Delta\lambda$) increases progressively over time, reaching a plateau at approximately 60 min. This plateau signifies the completion of the silver shell formation process: all available free $Ag^+$ has been reduced and deposited, and the nanostructure's optical properties have stabilized. Measurements taken before 60 min would capture the system in a transient, kinetically controlled state, leading to underestimation of the true analytical signal and poor reproducibility. Conversely, measurements taken beyond 60 min offer no analytical benefit, as the signal remains constant while unnecessarily extending the total assay time. Thus, 60 min was established as the optimal analysis time. This duration guarantees that the system has reached thermodynamic and optical equilibrium, ensuring maximum signal stability, reproducibility, and sensitivity. It also aligns with practical constraints, enabling a total assay time (including incubation and analysis) of approximately 90 min—a highly competitive timeframe for an instrument-free colorimetric biosensor.

## Quantitative performance

To establish the quantitative performance of the sensor, a series of *Salmonella typhimurium* suspensions at known concentrations were analyzed using the optimized sensing protocol. UV–Vis spectrophotometry revealed a progressive red shift in the longitudinal LSPR peak with increasing bacterial concentration, directly reflecting the dose-dependent inhibition of Ag shell formation on AuNRs (Fig. 5a). A linear calibration curve was constructed by plotting the LSPR peak shift ($\Delta\lambda = \lambda - \lambda_0$) against bacterial concentration (CFU $mL^{-1}$), yielding the equation: $Y = 0.45X + 108$ ($R^2 = 0.997$), where Y is the wavelength shift (nm) and X is the bacterial concentration ($\times 10^6$ CFU $mL^{-1}$) (Fig. 5b). The limit of detection (LOD) was calculated using the standard formula $LOD = 3\sigma/S$, where $\sigma$ is the standard deviation of ten blank measurements (no bacteria) and S is the slope of the calibration curve, resulting in an LOD of $2.0 \times 10^6$ CFU $mL^{-1}$. Critically, this quantitative spectral shift corresponds to distinct, naked-eye-visible color transitions—from orange-red through magenta, purple, and violet to teal—as bacterial concentration increases, enabling intuitive, instrument-free detection (Fig. 5c).

## Application in complex matrices

To evaluate the sensor's performance in complex real-world matrices, *Salmonella typhimurium* was detected in spiked samples of both chicken bouillon and tap water. The chicken bouillon matrix was prepared by dissolving a commercial bouillon cube in hot water, followed by filtration through qualitative filter paper to

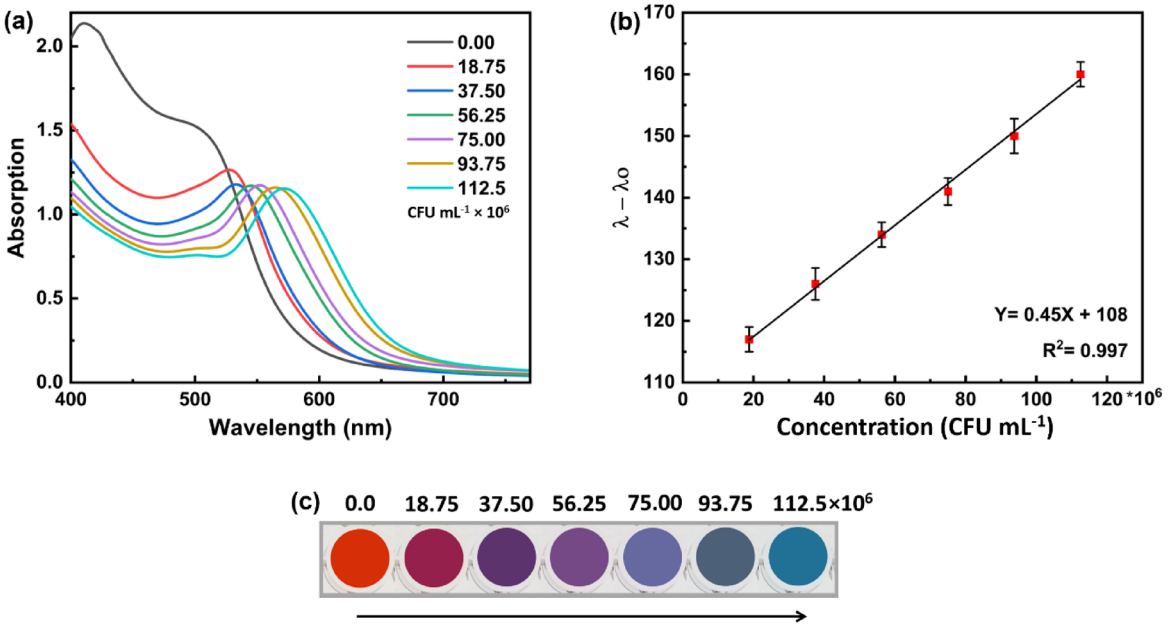


**Fig. 5**. Calibration and visual response of the sensor to *Salmonella typhimurium*. (**a**) UV–Vis absorption spectra showing progressive red shifts in the longitudinal LSPR peak with increasing bacterial concentrations ($18.75 \times 10^6$ to $112.5 \times 10^6$ CFU $mL^{-1}$), demonstrating inhibition of Au@AgNR shell formation. (**b**) Linear calibration curve correlating the LSPR peak shift ($\Delta\lambda = \lambda - \lambda_0$) with bacterial concentration (CFU $mL^{-1}$; $R^2 = 0.997$). (**c**) Representative color changes observed visually under optimized conditions, ranging from orange-red to teal as bacterial load increases.

| Sample | Initial concentration (CFU $mL^{-1}$) | Spiked (CFU $mL^{-1}$) | Found (CFU $mL^{-1}$) | Recovery (%) | RSD (%) |
|---|---|---|---|---|---|
| Chicken Bouillon | 0.0 | $75.0\times10^6$ | $70.0\times10^6$ | 93.3 | 3.5 |
| Tap Water | 0.0 | $75.0\times10^6$ | $72.0\times10^6$ | 96.0 | 2.5 |

**Table 1**. Detection of *Salmonella typhimurium* bacteria in real sample.

| NPs | Mechanism | Linear range (CFU $mL^{-1}$) | LOD (CFU $mL^{-1}$) | Analysis time (min) | Real sample | Estimated cost per test (USD) | Ref. |
|---|---|---|---|---|---|---|---|
| Streptavidin-coated AuNPs | SPR chip | $10^3$-$10^6$ | $7.4\times10^3$, $11.7\times10^3$ | 80 | Cucumber and Hamburger extracts | 25–30 | [59] |
| Magnetic AuNPs | Antibody-aptamer sandwich assay | $10^3$-$10^8$ | $10^3$ | 180 | Milk | 20–30 | [56] |
| TTC-functionalized $Fe_3O_4$-AuNCs | Enzymatic reaction | – | $10^8$ | 120 | – | 8–15 | [60] |
| $Fe_3O_4$ magnetic NPs | Enzymatic reaction | – | $7.5\times10^5$ | 10 | – | 3–6 | [61] |
| AuNPs | Lateral flow assay | $3\times10^5$-$3\times10^7$ | $3.0\times10^6$ | 10–15 | Milk | 5–10 | [58] |
| AuNPs | Aggregation | – | $6.6\times10^6$ | 10 | – | 1–3 | [57] |
| Label-free Au@AgNRs | Inhibited formation | $18.75\times10^6$-$112.5\times10^6$ | $2.0\times10^6$ | 90 | Chicken bouillon and Tap water | 1–3 | This work |

**Table 2**. The comparison of different colorimetric sensing systems on the basis of plasmonic and magnetic nanoparticles for the measurement of *Salmonella* bacteria.

remove insoluble particulates; tap water served as a low-complexity aqueous control. A known concentration of purified *Salmonella typhimurium* suspension was then added to each clarified matrix to achieve targeted spiking levels. After processing all samples through the full detection protocol—including immunomagnetic separation and colorimetric analysis—the recovery rates and relative standard deviations (RSD) were calculated to assess accuracy and precision. As summarized in Table 1, the system achieved recoveries of 93.3% (chicken bouillon) and 96.0% (tap water), with RSD values of 3.5% and 2.5%, respectively, demonstrating robust applicability, reliability, and minimal matrix interference under practical conditions.

Table 2 provides a comprehensive comparison of our sensor with previously reported plasmonic and magnetic nanoparticle-based colorimetric platforms for *Salmonella* detection. While our LOD is higher than enzyme-amplified or PCR-coupled methods[56], it is fully competitive—and in some cases superior—to other label-free, enzyme-free, visual-readout plasmonic sensors. Notably, our LOD is 3.3× lower than the aptamer-based AuNP aggregation sensor[57], 1.5× lower than the commercial lateral flow assay format[58]—despite our system being completely enzyme-free and requiring no gold nanoparticle surface modification. Unlike the highly sensitive surface plasmon resonance (SPR) biosensor[59]—which achieves a low LOD of $7.4\times10^3$ CFU $mL^{-1}$ through complex immobilization on functionalized chips and requires expensive optical instrumentation—our platform achieves acceptable sensitivity within a vastly simpler, instrument-free framework.

Beyond analytical performance, our platform offers distinct practical advantages as follows: (1) Low cost per test (~ 1.0–3.0 USD); our sensor is among the most cost-effective plasmonic platforms, leveraging inexpensive, unmodified AuNRs and common reagents—unlike antibody-conjugated systems[56,58] or enzymatic assays[60,61] that incur high reagent costs. (2) True visual readout with rainbow-like color transitions; Unlike most colorimetric assays that rely on binary red-to-blue shifts[57,58], our sensor produces a concentration-dependent spectral gradient (red → magenta → purple → violet → dark blue → teal), enabling semi-quantitative naked-eye estimation without instrumentation. (3) Minimal sample preparation complexity; While pre-enrichment is standard for all culture-compatible methods, our integrated magnetic separation using aptamer-MNPs streamlines sample-to-answer workflow—eliminating the need for antibody conjugation, enzymatic labeling, or nucleic acid extraction.

Within this framework, our platform's combination of low cost, visual readout, instrument-free operation, and compatibility with standard microbiological practice makes it uniquely suited for decentralized screening in resource-limited settings—where complex instrumentation, trained personnel, or expensive reagents are unavailable.

## Mechanistic basis of detection

Building upon the observed inhibition of Au@AgNR formation described in Sect. 3.1, we now dissect the molecular basis of this phenomenon to establish its validity as a specific recognition event. The core innovation of this work lies in transforming the innate biochemical interaction between *Salmonella typhimurium* and silver ions ($Ag^+$)—a phenomenon well-documented in microbial toxicology—into a quantifiable, visually interpretable optical signal. Unlike conventional biosensors that rely on antibody–antigen binding, aptamer hybridization, or enzymatic amplification, our platform exploits the passive, non-specific, yet highly reproducible adsorption and internalization of $Ag^+$ by bacterial surface biomolecules. This interaction serves as the primary recognition event, functionally replacing traditional biorecognition elements and enabling a label-free, enzyme-free detection paradigm. To elucidate the molecular underpinnings of this "anti-formation" mechanism, we

systematically dissect three critical stages: (i) the sequestration of $Ag^+$ by bacterial surface components, (ii) the quantitative inhibition of Au@Ag nanorod shell growth, and (iii) the role of magnetic pre-enrichment in conferring operational specificity.

*$Ag^+$ sequestration by bacterial surface biomolecules*

Upon exposure to $AgNO_3$, *Salmonella typhimurium* rapidly binds and internalizes silver ions through multivalent interactions with structurally abundant ligands on its Gram-negative envelope. The outer membrane, peptidoglycan layer, and periplasmic space are enriched with functional groups possessing high affinity for $Ag^+$. Thiol (–SH) groups in membrane proteins (e.g., thioredoxin, peroxiredoxins) and low-molecular-weight thiols (e.g., glutathione) form exceptionally stable linear Ag–S bonds, effectively immobilizing $Ag^+$ at the cell surface and within the periplasm[45]. Simultaneously, nitrogenous bases—particularly purines (adenine, guanine) and pyrimidines—in exposed extracellular DNA fragments, RNA, or nucleotide-binding domains coordinate with $Ag^+$ via N–Ag Lewis acid-base interactions, as validated in prior studies of Ag–DNA complexation[52–54]. Carboxylate ($–COO^-$) groups from lipopolysaccharides (LPS) and amine ($–NH_2$) groups in peptidoglycan subunits further contribute to ion trapping through electrostatic and coordination bonding[44,51]. Crucially, these interactions are not merely superficial; $Ag^+$ penetrates the porous peptidoglycan meshwork and accumulates in the periplasm, where it disrupts respiratory chain complexes (e.g., cytochrome oxidases) by displacing essential metal cofactors, inhibits ATP synthase by binding to proton channels, and induces oxidative stress by catalyzing Fenton-like reactions.

This multi-target sequestration depletes the free $Ag^+$ pool in solution in a concentration- and time-dependent manner, as confirmed by our optimization data (Fig. 4c, S3). Critically, this depletion is the triggering event for our sensing mechanism: the more $Ag^+$ is sequestered, the less remains available to be reduced and deposited onto AuNRs. We validated this directly using inductively coupled plasma mass spectrometry (ICP-MS), which demonstrated a dose-dependent decrease in supernatant $Ag^+$ concentration after bacterial incubation—providing unequivocal evidence that *Salmonella* acts as a biological sink for silver ions.

*Quantifiable Inhibition of core–shell formation*

In the absence of bacteria, ascorbic acid (AA) reduces $Ag^+$ ions homogeneously in solution, and the resulting $Ag^0$ atoms nucleate and grow epitaxially along the longitudinal axis of the AuNRs, forming a smooth, continuous, and conformal silver shell. This process increases the nanoparticle's overall diameter thereby reducing its aspect ratio—a geometric change that induces a large, reproducible blue shift (~100–150 nm) in the longitudinal LSPR peak (Fig. 3b, black spectrum). However, in the presence of *Salmonella*, the sequestered $Ag^+$ is no longer bioavailable for reduction. Consequently, the amount of $Ag^0$ generated during the 60-minute growth period is insufficient to fully coat the AuNRs. This leads to three interrelated outcomes: (i) Silver deposition becomes spatially heterogeneous, forming patchy, discontinuous, or island-like structures rather than a uniform shell; (ii) The underlying AuNR core retains a larger effective aspect ratio because its original dimensions are less masked by the incomplete silver overgrowth; and (iii) The resulting nanostructures exhibit a smaller degree of plasmonic coupling along their long axis, manifesting as a measurable red shift in the LSPR peak relative to the control (Fig. 3b, red spectrum). This red shift is not an artifact but a direct, proportional readout of the extent of $Ag^+$ sequestration: higher bacterial concentrations lead to greater $Ag^+$ depletion, more incomplete shells, and thus larger red shifts.

TEM imaging provides definitive structural confirmation: control samples show thick, uniform silver shells enveloping elongated rods (Fig. 3c), whereas samples with bacteria reveal thinner coatings with visible AuNR cores exposed (Fig. 3d). This "incomplete growth" phenomenon is the central transduction mechanism—it converts a biochemical event (ion binding) into a physical nanoscale modification (aspect ratio change) that is optically amplified and visually discernible.

*Magnetic pre-enrichment enables operational specificity*

While $Ag^+$ sequestration by bacterial surfaces is a general phenomenon observed across many Gram-negative species, our sensor achieves operational specificity for *Salmonella typhimurium* through an integrated, pre-analytical enrichment step: immunomagnetic separation using anti-Salmonella aptamer-conjugated Au/$Fe_3O_4$ magnetic nanoparticles (MNPs). This step ensures that only target cells—captured via high-affinity aptamer binding to Salmonella-specific surface antigens—are present during the critical $Ag^+$ incubation phase. Background microbiota (e.g., *E. coli*, *Listeria monocytogenes*) and matrix components (e.g., proteins, fats, particulates from chicken bouillon) are efficiently removed during magnetic washing, preventing them from contributing to non-specific $Ag^+$ binding or optical interference.

To rigorously quantify this selectivity, we evaluated the recovery efficiency of the MNP-based capture protocol against a panel of common foodborne pathogens. Equal suspensions (1000 CFU $mL^{-1}$) of *Escherichia coli*, *Staphylococcus aureus*, and *Listeria monocytogenes* were subjected to the same magnetic capture protocol optimized for *Salmonella typhimurium*. As shown in Table 3, the MNPs achieved a recovery rate of 85 ± 3% for *Salmonella typhimurium*, while exhibiting minimal cross-reactivity: 7 ± 1% for *E. coli*, 4 ± 1% for *Staphylococcus aureus*, and 3 ± 1% for *Listeria monocytogenes*. When normalized to *Salmonella* recovery (set at 100%), the relative responses were 8%, 5%, and 4%, respectively. These results demonstrate exceptional target specificity (> 90% discrimination over non-target species), confirming that the observed LSPR red shift originates exclusively from captured *Salmonella* cells and not from background flora or matrix interferents.

The near-complete absence of cross-reactivity validates that the sensor's specificity is conferred by the molecular recognition of aptamer–antigen interactions, not by inherent chemical affinity of $Ag^+$ for other bacteria. Thus, the magnetic pre-enrichment does not merely improve sensitivity; it transforms a non-specific biochemical interaction ($Ag^+$ binding) into a highly specific analytical signal by ensuring that the observed

| Bacterial species | Recovery efficiency (%) | Relative response (normalized to Salmonella %) |
|---|---|---|
| *Salmonella typhimurium* | 85 ± 3 | 100 |
| *Escherichia coli* | 7 ± 1 | 8 |
| *Staphylococcus aureus* | 4 ± 1 | 5 |
| *Listeria monocytogenes* | 3 ± 1 | 4 |

**Table 3**. Recovery efficiency and relative selectivity of the magnetic nanosensor towards *Salmonella typhimurium* and non-target bacteria (1000 CFU $mL^{-1}$).

LSPR response is attributable solely to the target pathogen. This integration of sample preparation and detection chemistry represents a paradigm shift: the sensor's specificity is engineered into the workflow itself, not the nanomaterial surface, making the platform robust, scalable, and suitable for real-world deployment.

## Conclusion

In summary, we presented a novel colorimetric sensor for *Salmonella typhimurium* that repurposes the bacterium's innate $Ag^+$ sequestration ability into a visual detection signal. By inhibiting the conformal growth of a silver shell on gold nanorods, bacterial presence induces a concentration-dependent red shift in the LSPR peak—accompanied by a vivid, naked-eye-distinguishable rainbow transition—enabling instrument-free, semi-quantitative detection. The platform achieves a limit of detection of $2.0 \times 10^6$ CFU $mL^{-1}$ and a linear range of $18.75–112.5 \times 10^6$ CFU $mL^{-1}$, outperforming many existing enzyme-free plasmonic sensors and rivaling commercial lateral flow assays—all without antibody conjugation or enzymatic amplification.

Crucially, integration with aptamer-functionalized magnetic nanoparticles enables specific capture from complex matrices (e.g., chicken bouillon), yielding > 93% recovery and minimal interference. This pre-enrichment step aligns with regulatory workflows (ISO/FDA) and is not a limitation, but a strategic advantage ensuring real-world applicability. With an estimated cost of $1–3 per test and no need for specialized equipment, our sensor offers unprecedented accessibility for decentralized screening in low-resource settings. It transforms a microbial defense mechanism into a simple, scalable diagnostic tool. While further reduction of the LOD remains a valuable objective for our future work, the current performance, robustness, and simplicity position this platform as a highly viable solution for immediate deployment in field-based food safety and public health screening programs.

## Data availability

The authors declare that the data supporting the findings of this study are available within the paper. Should any raw data files be needed in another format they are available from the corresponding author upon reasonable request.

Received: 7 July 2025; Accepted: 1 October 2025
Published online: 10 November 2025

## References

1. Ehuwa, O., Jaiswal, A. K. & Jaiswal, S. Salmonella, food safety and food handling practices. *Foods* **10**, 907. https://doi.org/10.3390/foods10050907 (2021).
2. Eng, S. K. et al. Salmonella: A review on pathogenesis, epidemiology and antibiotic resistance. *Front. Life Sci.* **8**, 284–293. https://doi.org/10.1080/21553769.2015.1051243 (2015).
3. Guerrero, T., Calderón, D., Zapata, S. & Trueba, G. Salmonella grows massively and aerobically in chicken faecal matter. *Microb. Biotechnol.* **13**, 1678–1684. https://doi.org/10.1111/1751-7915.13624 (2020).
4. Santiago, P. et al. High prevalence of *Salmonella* and *Enterococcus faecium* spp. In wastewater reused for irrigation assessed by molecular methods. *Int. J. Hyg. Environ Health*. **221**, 95–101. https://doi.org/10.1016/j.ijheh.2017.10.007 (2018).
5. Xie, Y. et al. Survivability of *Salmonella* and *Enterococcus faecium* in chili, cinnamon and black pepper powders during storage and isothermal treatments. *Food Control*. **137**, 108935. https://doi.org/10.1016/j.foodcont.2022.108935 (2022).
6. Sun, S. et al. Survival and thermal resistance of *Salmonella* in chocolate products with different water activities. *Food Res. Int.* **172**, 113209. https://doi.org/10.1016/j.foodres.2023.113209 (2023).
7. Sekhon, A. S. et al. Survival and thermal resistance of *Salmonella* in dry and hydrated nonfat dry milk and whole milk powder during extended storage. *Int. J. Food Microbiol.* **337**, 108950. https://doi.org/10.1016/j.ijfoodmicro.2020.108950 (2021).
8. Sithole, T. R., Ma, Y. X., Qin, Z., Wang, X. D. & Liu, H. M. Peanut butter food safety concerns—Prevalence, mitigation and control of *Salmonella* spp., and aflatoxins in peanut butter. *Foods* **11**, 1874. https://doi.org/10.3390/foods11131874 (2022).
9. Organization, W. H. *Salmonella (non-typhoidal)*, (2018).
10. Tokunaga, Y., Wakabayashi, Y., Yonogi, S. & Yamaguchi, N. Rapid quantification of *Escherichia coli* O157: H7 and *Salmonella typhimurium* in lettuce using immunomagnetic separation and a microfluidic system. *Biol. Pharm. Bull.* **47**, 1931–1936. https://doi.org/10.1248/bpb.b24-00352 (2024).
11. Konstantinou, L. et al. A Novel Application of B. EL. D™ Technology: Biosensor-based detection of Salmonella spp. in Food. *Biosensors* **14**, 582. https://doi.org/10.3390/bios14120582 (2024).
12. Van der Zee, H. Conventional methods for the detection and isolation of *Salmonella enteritidis*. *Int. J. Food Microbiol.* **21**, 41–46. https://doi.org/10.1016/0168-1605(94)90198-8 (1994).
13. Lee, K. M., Runyon, M., Herrman, T. J., Phillips, R. & Hsieh, J. Review of Salmonella detection and identification methods: Aspects of rapid emergency response and food safety. *Food Control*. **47**, 264–276. https://doi.org/10.1016/j.foodcont.2014.07.011 (2015).
14. Di Febo, T. et al. Development of a capture ELISA for rapid detection of *Salmonella enterica* in food samples. *Food. Anal. Methods*. **12**, 322–330. https://doi.org/10.1007/s12161-018-1363-2 (2019).

15. Rastawicki, W., Formińska, K. & Zasada, A. A. Development and evaluation of a latex agglutination test for the identification of *Francisella tularensis* subspecies pathogenic for human. *Pol. J. Microbiol.* **67**, 241. https://doi.org/10.21307/pjm-2018-030 (2018).
16. Kasturi, K. N. & Drgon, T. Real-time PCR method for detection of *Salmonella* spp. In environmental samples. *Appl. Environ. Microbiol.* **83**, e00644–e00617. https://doi.org/10.1128/AEM.00644-17 (2017).
17. Yu, S. et al. Rapid and sensitive detection of Salmonella in milk based on hybridization chain reaction and graphene oxide fluorescence platform. *J. Dairy Sci.* **104**, 12295–12302. https://doi.org/10.3168/jds.2021-20713 (2021).
18. Cai, Q. et al. Sensitive detection of Salmonella based on CRISPR-Cas12a and the tetrahedral DNA nanostructure-mediated hyperbranched hybridization chain reaction. *J. Agric. Food Chem.* **70**, 16382–16389. https://doi.org/10.1021/acs.jafc.2c05831 (2022).
19. Sun, J. et al. Rapid identification of *Salmonella serovars* by using Raman spectroscopy and machine learning algorithm. *Talanta* **253**, 123807. https://doi.org/10.1016/j.talanta.2022.123807 (2023).
20. Phothaworn, P., Meethai, C., Sirisarn, W. & Nale, J. Y. Efficiency of bacteriophage-based detection methods for non-Typhoidal Salmonella in foods: A systematic review. *Viruses* **16**, 1840. https://doi.org/10.3390/v16121840 (2024).
21. Yang, Q. et al. An overview of rapid detection methods for Salmonella. *Food Control* 110771. https://doi.org/10.1016/j.foodcont.2024.110771 (2024).
22. Wu, Y. et al. A microfluidic biosensor for quantitative detection of Salmonella in Traditional Chinese Medicine. *Biosensors* **15**, 10. https://doi.org/10.3390/bios15010010 (2024).
23. Putri, L. A. et al. Review of noble metal nanoparticle-based colorimetric sensors for food safety monitoring. *ACS Appl. Nano Mater.* **7**, 19821–19853. https://doi.org/10.1021/acsanm.4c04327 (2024).
24. Tang, L. & Li, J. Plasmon-based colorimetric nanosensors for ultrasensitive molecular diagnostics. *ACS Sens.* **2**, 857–875. https://doi.org/10.1021/acssensors.7b00282 (2017).
25. Ghasemi, F., Abbasi-Moayed, S., Ivrigh, Z. J. N. & Hormozi-Nezhad, M. R. in *Gold and Silver Nanoparticles* (eds Suban Sahoo & M. Reza Hormozi-Nezhad) 165–204 (Elsevier, 2023).
26. Koushkestani, M., Ghasemi, F. & Hormozi-Nezhad, M. R. Ratiometric dual-mode optical sensor array for the identification and differentiation of pesticides in vegetables with mixed plasmonic and fluorescent nanostructures. *ACS Appl. Nano Mater.* **7**, 2764–2774. https://doi.org/10.1021/acsanm.3c04982 (2024).
27. Olson, J. et al. Optical characterization of single plasmonic nanoparticles. *Chem. Soc. Rev.* **44**, 40–57. https://doi.org/10.1039/C4CS00131A (2015).
28. Liu, J. et al. Recent advances of plasmonic nanoparticles and their applications. *Materials* **11**, 1833. https://doi.org/10.3390/ma11101833 (2018).
29. Taefi, Z., Ghasemi, F. & Hormozi-Nezhad, M. R. Selective colorimetric detection of pentaerythritol tetranitrate (PETN) using arginine-mediated aggregation of gold nanoparticles. *Spectrochim. Acta Part A Mol. Biomol. Spectrosc.* **228**, 117803. https://doi.org/10.1016/j.saa.2019.117803 (2020).
30. Mohammadi, A., Ghasemi, F. & Hormozi-Nezhad, M. R. Development of a paper-based plasmonic test strip for visual detection of methiocarb insecticide. *IEEE Sens. J.* **17**, 6044–6049. https://doi.org/10.1109/JSEN.2017.2731418 (2017).
31. Sepahvand, M., Ghasemi, F. & Hosseini, H. M. S. Thiol-mediated etching of gold nanorods as a neoteric strategy for room-temperature and multicolor detection of nitrite and nitrate. *Anal. Methods*. **13**, 4370–4378. https://doi.org/10.1039/D1AY01117K (2021).
32. Abdali, M., Ghasemi, F., Hosseini, S., Mahdavi, V. & H. M. & Different sized gold nanoparticles for array-based sensing of pesticides and its application for strawberry pollution monitoring. *Talanta* **267**, 125121. https://doi.org/10.1016/j.talanta.2023.125121 (2024).
33. Hemmati, M., Selakjan, A. H. Q. & Ghasemi, F. Iron (III) edta-accelerated growth of gold/silver core/shell nanoparticles for wide-range colorimetric detection of hydrogen peroxide. *Sci. Rep.* **15**, 4050. https://doi.org/10.1038/s41598-025-88342-4 (2025).
34. Chen, J., Jackson, A. A., Rotello, V. M. & Nugen, S. R. Colorimetric detection of *Escherichia coli* based on the enzyme-induced metallization of gold nanorods. *Small* **12**, 2469–2475. https://doi.org/10.1002/smll.201503682 (2016).
35. Zhao, P., Li, N. & Astruc, D. State of the Art in gold nanoparticle synthesis. *Coord. Chem. Rev.* **257**, 638–665. https://doi.org/10.1016/j.ccr.2012.09.002 (2013).
36. Sahu, A. K., Das, A., Ghosh, A. & Raj, S. Understanding blue shift of the longitudinal surface plasmon resonance during growth of gold nanorods. *Nano Express*. **2**, 010009. https://doi.org/10.48550/arXiv.2106.06365 (2021).
37. Awiaz, G., Lin, J. & Wu, A. Recent advances of Au@Ag core–shell SERS-based biosensors. *Exploration* **3**, 20220072. https://doi.org/10.1002/EXP.20220072 (2023).
38. Lu, L., Burkey, G., Halaciuga, I. & Goia, D. V. Core–shell gold/silver nanoparticles: Synthesis and optical properties. *J. Colloid Interface Sci.* **392**, 90–95. https://doi.org/10.1016/j.jcis.2012.09.057 (2013).
39. Ghorbanian, E., Ghasemi, F., Tavabe, K. R. & Sabet, H. R. A. Formation of plasmonic core/shell nanorods through ammonia-mediated dissolution of silver (I) oxide for ammonia monitoring. *Nanoscale Adv.* **6**, 3229–3238. https://doi.org/10.1039/D4NA00216D (2024).
40. Naseri, A. & Ghasemi, F. Analyte-restrained silver coating of gold nanostructures: an efficient strategy to advance multicolorimetric probes. *Nanotechnology* **33**, 075501. https://doi.org/10.1088/1361-6528/ac3704 (2021).
41. Orouji, A., Ghasemi, F. & Hormozi-Nezhad, M. R. Machine learning-assisted colorimetric assay based on Au@ ag nanorods for chromium speciation. *Anal. Chem.* **95**, 10110–10118. https://doi.org/10.1021/acs.analchem.3c01904 (2023).
42. Shirzad, M., Anbarestani, M. & Ghasemi, F. Ion-mediated etching of Au–Ag core-shell nanorods for LSPR-based discrimination of hazardous ions. *Anal. Chim. Acta*. **1357**, 344066. https://doi.org/10.1016/j.aca.2025.344066 (2025).
43. Sepahvand, M. & Ghasemi, F. Colorimetric silver ion detection based on silver metallization of gold nanorods. *ChemistrySelect* **9** (e202400080). https://doi.org/10.1002/slct.202400080 (2024).
44. Slawson, R., Lee, H. & Trevors, J. Bacterial interactions with silver. *Biology Met.* **3**, 151–154. https://doi.org/10.1007/BF01140573 (1990).
45. Jung, W. K. et al. Antibacterial activity and mechanism of action of the silver ion in Staphylococcus aureus and Escherichia coli. *Appl. Environ. Microbiol.* **74**, 2171–2178. https://doi.org/10.1128/AEM.02001-07 (2008).
46. Hamad, A., Khashan, K. S. & Hadi, A. Silver nanoparticles and silver ions as potential antibacterial agents. *J. Inorg. Organomet. Polym Mater.* **30**, 4811–4828. https://doi.org/10.1007/s10904-020-01744-x (2020).
47. Scarabelli, L., Grzelczak, M. & Liz-Marzán, L. M. Tuning gold Nanorod synthesis through prereduction with Salicylic acid. *Chem. Mater.* **25**, 4232–4238. https://doi.org/10.1021/cm402177b (2013).
48. Miryousefi, N., Varmazyad, M. & Ghasemi, F. Synthesis of Au@Ag core-shell nanorods with tunable optical properties. *Nanotechnology* **35**, 395605. https://doi.org/10.1088/1361-6528/ad572b (2024).
49. Randall, C. P., Gupta, A., Jackson, N., Busse, D. & O'Neill, A. J. Silver resistance in Gram-negative bacteria: a dissection of endogenous and exogenous mechanisms. *J. Antimicrob. Chemother.* **70**, 1037–1046. https://doi.org/10.1093/jac/dku523 (2015).
50. Terzioğlu, E., Arslan, M., Balaban, B. G. & Çakar, Z. P. Microbial silver resistance mechanisms: recent developments. *World J. Microbiol. Biotechnol.* **38**, 158. https://doi.org/10.1007/s11274-022-03341-1 (2022).
51. Rieger, K. A., Cho, H. J., Yeung, H. F., Fan, W. & Schiffman, J. D. Antimicrobial activity of silver ions released from zeolites immobilized on cellulose nanofiber Mats. *ACS Appl. Mater. Interfaces*. **8**, 3032–3040. https://doi.org/10.1021/acsami.5b10130 (2016).
52. Bragg, P. & Rainnie, D. The effect of silver ions on the respiratory chain of Escherichia coli. *Can. J. Microbiol.* **20**, 883–889. https://doi.org/10.1139/m74-135 (1974).

53. Furr, J. R., Russell, A., Turner, T. & Andrews, A. Antibacterial activity of actisorb Plus, actisorb and silver nitrate. *J. Hosp. Infect.* **27**, 201–208. https://doi.org/10.1016/0195-6701(94)90128-7 (1994).
54. Yakabe, Y., Sano, T., Ushio, H. & Yasunaga, T. Kinetic studies of the interaction between silver ion and deoxyribonucleic acid. *Chem. Lett.* **9**, 373–376. https://doi.org/10.1246/cl.1980.373 (1980).
55. Gruen, L. C. Interaction of amino acids with silver (I) ions. *Biochim. Et Biophys. Acta (BBA)-Protein Struct.* **386**, 270–274. https://doi.org/10.1016/0005-2795(75)90268-8 (1975).
56. Wu, W. et al. Gold nanoparticle-based enzyme-linked antibody-aptamer sandwich assay for detection of *Salmonella typhimurium*. *ACS Appl. Mater. Interfaces*. **6**, 16974–16981. https://doi.org/10.1021/am5045828 (2014).
57. Du, J. et al. A low pH-based rapid and direct colorimetric sensing of bacteria using unmodified gold nanoparticles. *J. Microbiol. Methods*. **180**, 106110. https://doi.org/10.1016/j.mimet.2020.106110 (2021).
58. Yahaya, M. L., Zakaria, N. D., Noordin, R. & Abdul Razak, K. Development of rapid gold nanoparticles based lateral flow assays for simultaneous detection of Shigella and Salmonella genera. *Biotechnol. Appl. Chem.* **68**, 1095–1106. https://doi.org/10.1002/bab.2029 (2021).
59. Vaisocherová-Lísalová, H. et al. Low-fouling surface plasmon resonance biosensor for multi-step detection of foodborne bacterial pathogens in complex food samples. *Biosens. Bioelectron.* **80**, 84–90. https://doi.org/10.1016/j.bios.2016.01.040 (2016).
60. Daramola, O. B., Torimiro, N. & George, R. C. Colorimetric-based detection of enteric bacterial pathogens using chromogens-functionalized iron oxide-gold nanocomposites biosynthesized by *Bacillus subtilis*. *Discover Biotechnol.* **2**, 1. https://doi.org/10.1007/s44340-025-00008-z (2025).
61. Park, J. Y., Jeong, H. Y., Kim, M. I. & Park, T. J. Colorimetric detection system for *Salmonella typhimurium* based on peroxidase-like activity of magnetic nanoparticles with DNA aptamers. *J. Nanomater.* 527126 (2015). https://doi.org/10.1155/2015/527126 (2015).


## Author contributions

S.S.: Investigation, Methodology; A.H.Q.S: Validation, Writing – original draft, F.G.: Conceptualization, Resources, Supervision, Writing – review and editing; E.S.: Resources, Validation, Writing – review and editing; P.K.Z.: Investigation; M.A.: Validation.

## Declarations

## Competing interests

The authors declare no competing interests.

## Additional information

**Supplementary Information** The online version contains supplementary material available at https://doi.org/10.1038/s41598-025-22852-z.

**Correspondence** and requests for materials should be addressed to F.G.

**Reprints and permissions information** is available at www.nature.com/reprints.

**Publisher's note** Springer Nature remains neutral with regard to jurisdictional claims in published maps and institutional affiliations.